SUPPLEMENTARY MATERIALS

Chirality and Ultra-Fast Laser Irradiation

Xiao Peng Mi[1], Hui Lu[1], Tianlv Xu[1], Herbert Früchtl[2], Tanja van Mourik[2], Martin, J. Paterson[3], Steven R. Kirk[*1] and Samantha Jenkins[*1]

[1]Key Laboratory of Chemical Biology and Traditional Chinese Medicine Research and Key Laboratory of Resource National and Local Joint Engineering Laboratory for New Petro-chemical Materials and Fine Utilization of Resources, College of Chemistry and Chemical Engineering, Hunan Normal University, Changsha, Hunan 410081, China
[2]EaStCHEM School of Chemistry, University of Saint Andrews, North Haugh, St Andrews, Fife KY16 9ST, Scotland, United Kingdom.
[3]Institute of Chemical Sciences, School of Engineering and Physical Sciences, Heriot-Watt University, Edinburgh, EH14 4AS, UK

email: steven.kirk@cantab.net
email: samanthajsuman@gmail.com

1. Supplementary Materials S1. NG-QTAIM theoretical background and procedure to generate the Hessian of $\rho(\mathbf{r})$ trajectories $\mathbb{T}(s)$.

2. Supplementary Materials S2. Tabulated Excitation frequencies ω.

3. Supplementary Materials S3. Populations for an excitation frequency ω = 0.350 a.u. and plane of circular laser pulse polarization *xy*.

4. Supplementary Materials S4. Populations for an excitation frequency ω = 0.350 a.u. and plane of circular laser pulse polarization *xz*.

5. Supplementary Materials S5. Populations for an excitation frequency ω = 0.350 a.u. and plane of circular laser pulse polarization *yz*.

6. Supplementary Materials S6. Variations of the ethane C1-C2 *BCP* ellipticity ε for the right-handed (CW, [+1]) and left-handed (CCW, [-1]) circularly polarized laser pulse polarized in the *xz, xy* and *yz* planes.

7. Supplementary Materials S7. Maximum Hessian of $\rho(\mathbf{r})$ trajectory projections $\mathbb{T}_{max}(\boldsymbol{s})$ tables for the C1-C2 *BCP*s.

1. Supplementary Materials S1. NG-QTAIM theoretical background and procedure to generate the Hessian of $\rho(\mathbf{r})$ trajectories $\mathbb{T}(s)$.

1(a) *QTAIM bond critical point (BCP) properties; ellipticity ε:*

The four types of QTAIM critical points are labeled using the notation (R, ω) where R is the rank of the Hessian matrix, i.e., the number of distinct non-zero eigenvalues and ω is the signature (the algebraic sum of the signs of the eigenvalues); the (3, -3) [nuclear critical point (*NCP*), a local maximum], (3, -1) and (3, 1) [saddle points, referred to as bond critical points (*BCP*) and ring critical points (*RCP*), respectively] and (3, 3) [the cage critical points (*CCP*)]. In the limit that the forces on the nuclei are zero, an atomic interaction line[1] the line passing through a *BCP* and terminating on two nuclear attractors along which the charge density $\rho(\mathbf{r})$ is locally maximal with respect to nearby lines, becomes a bond-path[2]. The full set of critical points with the bond-paths of a molecule or cluster is referred to as the molecular graph.

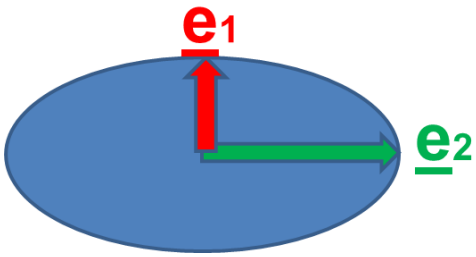

Scheme S1. The cross section through a bond at the bond critical point (*BCP*). The λ_1 and λ_2 eigenvalues with associated eigenvectors $\underline{\mathbf{e}}_1$ and $\underline{\mathbf{e}}_2$ respectively, define the axes of the ellipse and indicate the magnitudes of the least and greatest extents of the distribution of $\rho(\mathbf{r})$.

The ellipticity, ε, defined as $\varepsilon = |\lambda_1|/|\lambda_2| - 1$, quantifies the relative accumulation of the electronic charge density $\rho(\mathbf{r_b})$ distribution in the two directions $\underline{\mathbf{e}}_1$ and $\underline{\mathbf{e}}_2$ that are perpendicular to the bond-path at a Bond Critical Point (*BCP*) with position $\mathbf{r_b}$. For ellipticity $\varepsilon > 0$, the shortest and longest axes of the elliptical distribution of $\rho(\mathbf{r_b})$ are associated with the λ_1 and λ_2 eigenvalues, respectively. From the electron-preceding perspective a change in the electronic charge density distribution that defines a chemical bond causes in a change in atomic positions[3]. Bone and Bader later proposed that the direction of motion of the atoms that results from a slightly perturbed structure coincides with the direction of motion of the electrons[4]; this was later confirmed[5], [6].

1(b) *QTAIM bond-path properties; bond-path length (BPL)* **:**

The bond-path length (BPL) is defined as the length of the path traced out by the $\underline{\mathbf{e}}_3$ eigenvector of the Hessian of the total charge density $\rho(\mathbf{r})$, passing through the *BCP*, along which $\rho(\mathbf{r})$ is locally maximal with respect to any neighboring paths. The bond-path curvature separating two bonded nuclei is defined as the dimensionless ratio

(BPL - GBL)/GBL, where the BPL is defined to be the bond-path length associated and GBL is the inter-nuclear separation. The BPL often exceeds the GBL particularly in strained bonding environments[5]. Earlier, one of the current authors hypothesized that a bond-path may possess 1-D, 2-D or a 3-D morphology[7], with 2-D or a 3-D bond-paths associated with a *BCP* with ellipticity $\varepsilon > 0$, being due to the differing degrees of charge density accumulation, of the λ_2 and λ_1 eigenvalues respectively. Bond-paths possessing zero and non-zero values of the bond-path curvature defined by equation **(2)** can be considered to possess 1-D and 2-D topologies respectively. We start by choosing the length traced out in 3-D by the path swept by the tips of the scaled $\underline{\mathbf{e}}_2$ eigenvectors of the λ_2 eigenvalue, the scaling factor being chosen as the ellipticity ε, see **Scheme S1**.

Full Symmetry-breaking for Iso-Energetic Phenomena: Derivation and numerical procedure of the second-generation eigenvector-space trajectory $\mathbb{T}_i(\boldsymbol{s})$

1(a) *The Second-Generation eigenvector-space trajectories*: $\mathbb{T}_i(\boldsymbol{s})$; $i = \{\rho\}$ *for Stereochemistry:*

The maximum eigenvector projections $\mathbb{T}(\boldsymbol{s})_{\mathbf{max}} = \{t_{1\mathbf{max}}, t_{2\mathbf{max}}, t_{3\mathbf{max}}\}$ are used to define the dimensions of a 'bounding box' around each $\mathbb{T}(\boldsymbol{s})$ and are used to calculate the chirality $\mathbb{C}$, bond-flexing $\mathbb{F}$ and bond-axiality $\mathbb{B}$. The subscript '$_{\mathbf{max}}$' corresponds to the difference between the minimum and maximum value of the projection of the *BCP* shift **dr** onto $\underline{\mathbf{e}}_1$, $\underline{\mathbf{e}}_2$ or $\underline{\mathbf{e}}_3$ along the entire $\mathbb{T}(\boldsymbol{s})$. Note: the $\mathbf{e}_2$ corresponds to the direction in which the electrons at the *BCP* are subject to the most compressive forces[8], therefore $\mathbf{e}_2$ corresponds to the most *facile direction* for displacement of the *BCP* electrons when the *BCP* is torsioned. Conversely the $\mathbf{e}_1$ and $\mathbf{e}_3$ correspond to the directions associated with the least compressive forces and the tensile forces on the *BCP* electrons respectively.

The chirality $\mathbb{C}$ is generated from the $\boldsymbol{t}_2 = \underline{\mathbf{e}}_2 \cdot \mathbf{dr}$ (bond-twist) *BCP* shift in the plane perpendicular to $\underline{\mathbf{e}}_3$ (the bond-path) and is defined by the difference in the maximum $\mathbb{T}(\boldsymbol{s})$ projections (the dot product of the eigenvector $\underline{\mathbf{e}}_2$ eigenvector and the *BCP* shift **dr**) of the $\mathbb{T}(\boldsymbol{s})$ values between the CCW and CW torsions:

$$\mathbb{C} = [(\underline{\mathbf{e}}_2 \cdot \mathbf{dr})_{\mathbf{max}}]_{\mathrm{CCW}} - [(\underline{\mathbf{e}}_2 \cdot \mathbf{dr})_{\mathbf{max}}]_{\mathrm{CW}} \qquad \textbf{(S1.1)}$$

The bond-flexing $\mathbb{F}$ is generated from $\boldsymbol{t}_1 = \underline{\mathbf{e}}_1 \cdot \mathbf{dr}$ where $\underline{\mathbf{e}}_1$ corresponds to the least facile Hessian of $\rho(\mathbf{r})$ eigenvector:

$$\mathbb{F} = [(\underline{\mathbf{e}}_1 \cdot \mathbf{dr})_{\mathbf{max}}]_{\mathrm{CCW}} - [(\underline{\mathbf{e}}_1 \cdot \mathbf{dr})_{\mathbf{max}}]_{\mathrm{CW}} \qquad \textbf{(S1.2)}$$

The bond-axiality $\mathbb{A}$ is generated from the axial *BCP* sliding $t_3 = \underline{e}_3 \cdot \mathbf{dr}$[9], where the *BCP* sliding is the shift of the *BCP* position along the containing bond-path:

$$\mathbb{A} = [(\underline{e}_3 \cdot \mathbf{dr})_{max}]_{CCW} - [(\underline{e}_3 \cdot \mathbf{dr})_{max}]_{CW} \qquad \textbf{(S1.3)}$$

and quantifies the resultant extent of *axial* displacement of the *BCP* in response to the bond torsion (CCW vs. CW), i.e. the sliding of the *BCP* along the bond-path[9].

The sign (+) or (-) of each of the chirality $\mathbb{C}$, bond-flexing $\mathbb{F}$ and bond-axiality $\mathbb{A}$ from equations **(S1.1)-(S1.3)** respectively determines the presence of **S** character for $\mathbb{C} > 0$, $\mathbb{F} > 0$ or $\mathbb{A} > 0$ and **R** character for $\mathbb{C} < 0$, $\mathbb{F} < 0$ or $\mathbb{A} < 0$. The complete set {bond-flexing $\mathbb{F}$, chirality $\mathbb{C}$, bond axiality $\mathbb{A}$} is referred to as the *distortion* set.

A helical response of the $\rho(\mathbf{r_b})$ both non-axial, perpendicular to the bond-path and axial (parallel to the bond-path) displacements of the torsional C1-C2 *BCP* may be found, see the helical shaped $\mathbb{T}(s)$. The circumstances that lead to helical or linear trajectories $\mathbb{T}(s)$ are not limited to chiral molecules, but also apply to formally achiral molecules that have the capacity to become chiral when subject to suitable substitution. The chirality-helicity function $\mathbb{C}_{helicity}$ is the arithmetic product of the circular ($\mathbb{C}$) and the magnitude of the axial ($\mathbb{A}$) displacement and consequently quantifies the resultant displacement of the torsional *BCP*:

$$\mathbb{C}_{helicity} = (\text{chirality } \mathbb{C}) \times (|\text{axiality } \mathbb{A}|) = \mathbb{C}|\mathbb{A}| \qquad \textbf{(S1.4)}$$

2(b) *Numerical Considerations for Calculation of the Second-Generation Eigenvector-Space Trajectory* $\mathbb{T}_i(s)$

Central to the concept of the second-generation eigenvector-space trajectory $\mathbb{T}_i(s)$ is the concept of a monotonically increasing sequence parameter s, which may take the form of an increasing integer sequence (0, 1, 2, 3,...) in applications where a set of discrete numbered steps are involved, or a continuous real number. The 3-D eigenvector trajectory $\mathbb{T}_i(s)$ is then defined as an ordered set of points, whose sequence is described by the parameter s. In this application, we used an integer step number for s. We first choose to associate $s = 0$ with a specific reference molecular graph, in this case, the energy minimum structure. For a specific *BCP*, the coordinates associated with each of the points are calculated by evaluating the components of the shift vector **dr**

= $\mathbf{r}_b(s) - \mathbf{r}_b(s\text{-}1)$ where $\mathbf{r}_b$ indicates the location of the *BCP*, from the previous step to the current step in the reference coordinate frame defined by the eigenvectors $\underline{\mathbf{e}}_1$, $\underline{\mathbf{e}}_2$, $\underline{\mathbf{e}}_3$.

Note: for displaying the eigenvector trajectories $\mathbb{T}_i(s)$, large steps that can occur at the beginning or end of a $\mathbb{T}_i(s)$ may swamp the appearance of the $\mathbb{T}_i(s)$. To solve this we temporarily filter these steps before including them back in to correctly calculate the $\mathbb{U}_\sigma$-space eigenvector trajectory $\mathbb{T}_i(s)$.

The calculation of the $\mathbb{T}_i(s)$ is made easier if the code which produces the list of structures corresponding to points along each step of the torsion (CW) and counterclockwise CCW generates these structures at regularly-spaced points. The consequence of this desirable characteristic is that there are few or no large changes or 'spikes' in the magnitude of the *BCP* shift vector **dr** i.e. $\Delta\mathbf{dr}$, between path step s and $s + 1$. Such anomalies occur because some path-following algorithms may employ occasional small predictor-corrector steps that are at least an order of magnitude smaller than standard steps. In this analysis it is observed that such intermittent relatively small steps in turn cause very small shifts **dr** to be interspersed between longer runs of larger changes, causing 'spike' noise in the otherwise smooth trajectories $\mathbb{T}_i(s)$. Such 'spikes', which usually only consist of a single spurious point deviating from the locally smooth eigenvector trajectory, can make potentially large spurious contributions to the eigenvector trajectory $\mathbb{T}_i(s)$ and may be safely filtered. A combination of criteria are recommended for automated rejection of inclusion of a specific point into the trajectories $\mathbb{T}_i(s)$:

1. If the magnitude of the **dr** associated with any current $\mathbb{T}_i(s)$ point is less than 50% of the average of the corresponding **dr** values associated with the immediately preceding point and the immediately following point, the current point is filtered out as a ‘spike’.
2. Abrupt changes in direction in the $\mathbb{T}_i(s)$, e.g. turning by more than 60^0 from one $\mathbb{T}_i(s)$ step to the next cause the current point to be labelled as a ‘spike’.

These two rules taken together are referred to as the ‘turn’ filter. These rules can be repeatedly applied across multiple ‘passes’ through the eigenvector trajectory data as necessary.

It has been observed that the magnitudes of the steps **dr** naturally tend to slowly decrease toward the end of paths, corresponding to a slowed approach to an end minimum, and the corresponding part of the $\mathbb{T}_i(s)$ turns toward the $\mathbb{U}_i$-space origin. A combination of the criteria mentioned above may be deployed to retain these parts of the $\mathbb{T}_i(s)$.

An alternative Kolmogorov-Zurbenko[10] data ‘smoothing’ filter may also be applied.

References

[1] R. F. W. Bader, *J. Phys. Chem. A*, **1998**, DOI:10.1021/jp981794v.

[2] R. F. W. Bader, *J. Phys. Chem. A*, **2009**, DOI:10.1021/jp906341r.
[3] H. Nakatsuji, *J. Am. Chem. Soc.*, **1974**, DOI:10.1021/ja00808a004.
[4] R. G. A. Bone, R. F. W. Bader, *J. Phys. Chem.*, **1996**, DOI:10.1021/jp953512m.
[5] S. Jenkins, M. I. Heggie, *J. Phys. Condens. Matter*, **2000**, DOI:10.1088/0953-8984/12/49/3.
[6] P. W. Ayers, S. Jenkins, *J. Chem. Phys.*, **2009**, DOI:10.1063/1.3098140.
[7] S. Jenkins, I. Morrison, *Chem. Phys. Lett.*, **2000**, DOI:10.1016/S0009-2614(99)01306-8.
[8] P. Szarek, Y. Sueda, A. Tachibana, *J. Chem. Phys.*, **2008**, DOI:10.1063/1.2973634.
[9] T. Tian, T. Xu, S. R. Kirk, I. T. Rongde, Y. B. Tan, S. Manzhos, Y. Shigeta, S. Jenkins, *Phys. Chem. Chem. Phys.*, **2020**, DOI:10.1039/C9CP05879F.
[10] W. Yang, I. Zurbenko, *Wiley Interdiscip. Rev. Comput. Stat.*, **2010**, DOI:10.1002/wics.71.

2. Supplementary Materials S2. Tabulated Excitation frequencies ω.

Table S2. Excitation frequencies ω for excited states from initial time dependent density functional theory (TDDFT) zero electric field calculations in atomic units (au).

Electronic State	Excitation frequency ω (a.u)
S_0	0.0000000
S_1	0.3173230
S_2	0.3173230
S_3	0.3433195
S_4	0.3433195
S_5	0.3473178
S_6	0.3506694
S_7	0.3506694
S_8	0.3521798
S_9	0.3531169
S_{10}	0.3729211
S_{11}	0.3787348
S_{12}	0.3787348
S_{13}	0.3822995
S_{14}	0.3822995
S_{15}	0.3828067
S_{16}	0.3849051
S_{17}	0.3861545
S_{18}	0.3861582
S_{19}	0.3999760
S_{20}	0.4037758

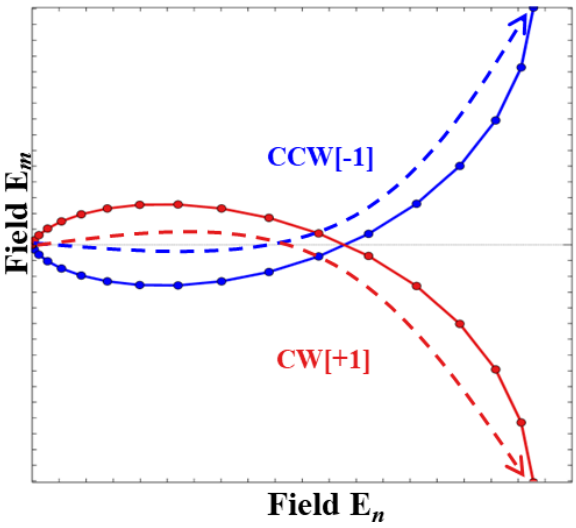

Scheme S2. A sketch of the first seventeen steps demonstrating the left-handed counter-clockwise (CCW [-1]) and right-handed clockwise (CW [+1]) character of the time evolution of the electric field $\mathbf{E}_n$ and $\mathbf{E}_m$ components in the $\boldsymbol{n}$, $\boldsymbol{m}$ $\{\boldsymbol{n}, \boldsymbol{m} = (x,y), (x,z)$ and $(y,z)\}$ planes of the applied ultra-fast laser pulse corresponding to the CCW (blue) and CW (red) circular polarizations. The blue and red dashed arrows both indicate increasing time. For further details see **Scheme 1**.

3. Supplementary Materials S3. Populations for an excitation frequency ω = 0.350 a.u. and plane of circular laser pulse polarization *xy*.

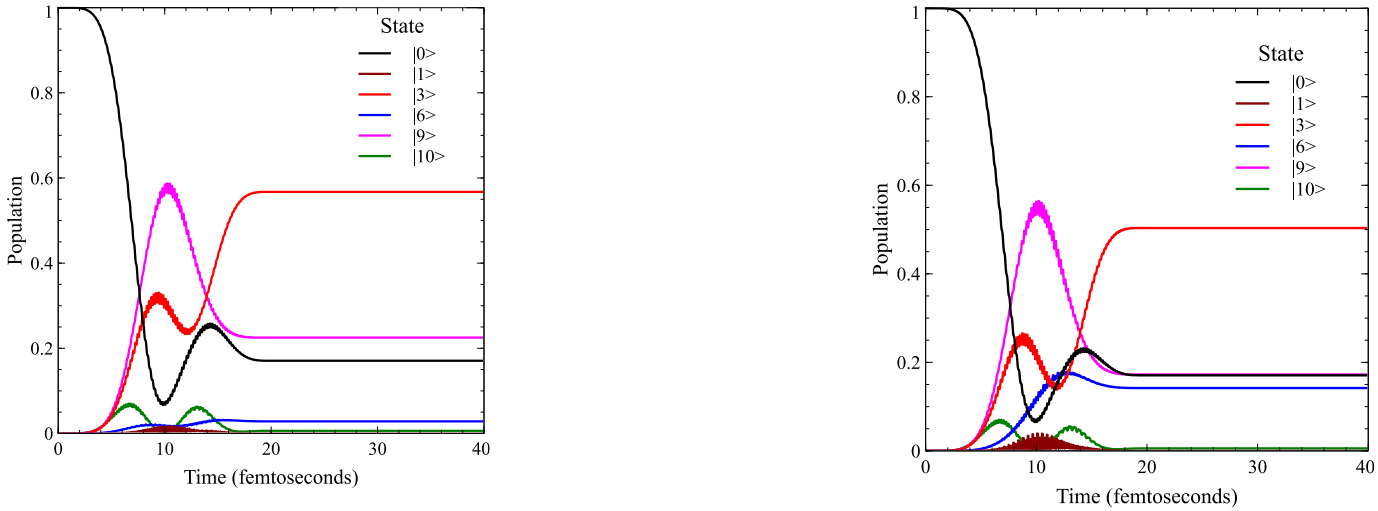

Figure S3(a). The variations of population of electronic states for the clockwise (CW) (left-panel) and counterclockwise (CCW) (right-panel) that are non-zero for the plane of circular laser pulse polarization *xy*. Pulses are 20 fs long and have a 'sin^2' amplitude envelope with peak field magnitude 0.02 au. Both the basic laser frequency oscillation and the pulse envelope start with phase = 0 at time t = 0 fs. Note that after t = 40 fs, populations remain constant until the end of the dynamics run at t = 100 fs. Only the states which exceed a population of 0.05 or greater at any point in the dynamics are shown.

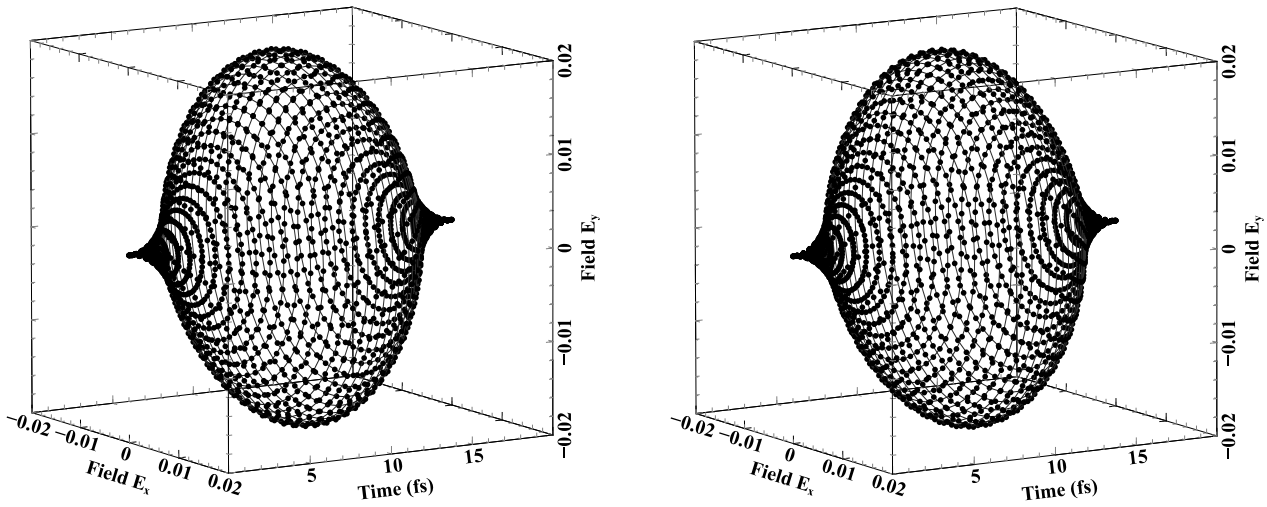

Figure S3(b). Time variations of the laser pulse electric field components $\mathbf{E}_x$, $\mathbf{E}_y$ for the *xy*-plane circular laser pulse polarization: clockwise (CW) (left-panel) and counterclockwise (CCW) (right-panel).

4. Supplementary Materials S3. Populations for an excitation frequency ω = 0.350 a.u. and plane of circular laser pulse polarization *xz*.

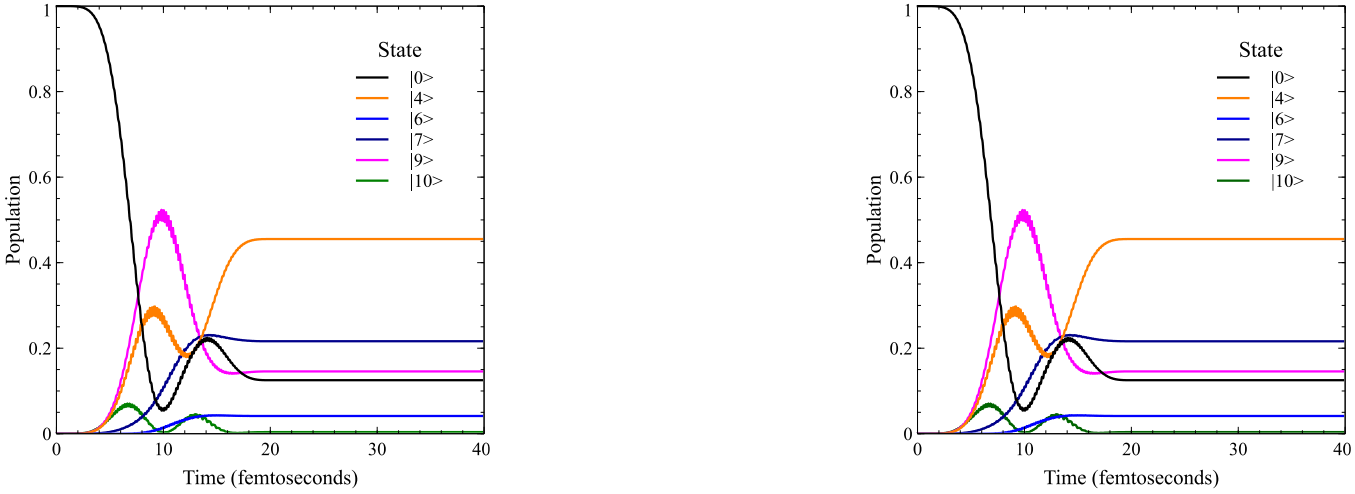

Figure S4(a). The variations of population with time of significantly populated electronic states for the clockwise (CW) (left-panel) and counterclockwise (CCW) (right-panel) *xz*-plane circularly polarized at t = 20 fs '$\sin^2$' simulated laser pulses. See the caption of **Figure 3(a)** for further details.

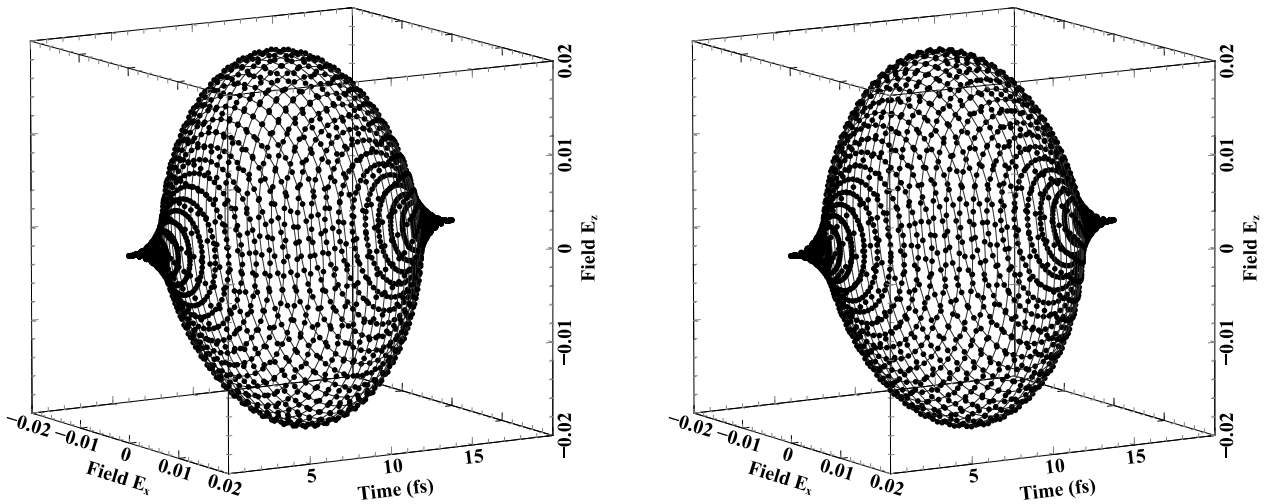

.

Figure S4(b). Time variations of the laser pulse electric field components $\mathbf{E}_x$, $\mathbf{E}_z$ for the *xz*-plane circular laser pulse polarization: clockwise (CW) (left-panel) and counterclockwise (CCW) (right-panel).

5. Supplementary Materials S5. Populations for an excitation frequency ω = 0.350 a.u. and plane of circular laser pulse polarization *yz***.**

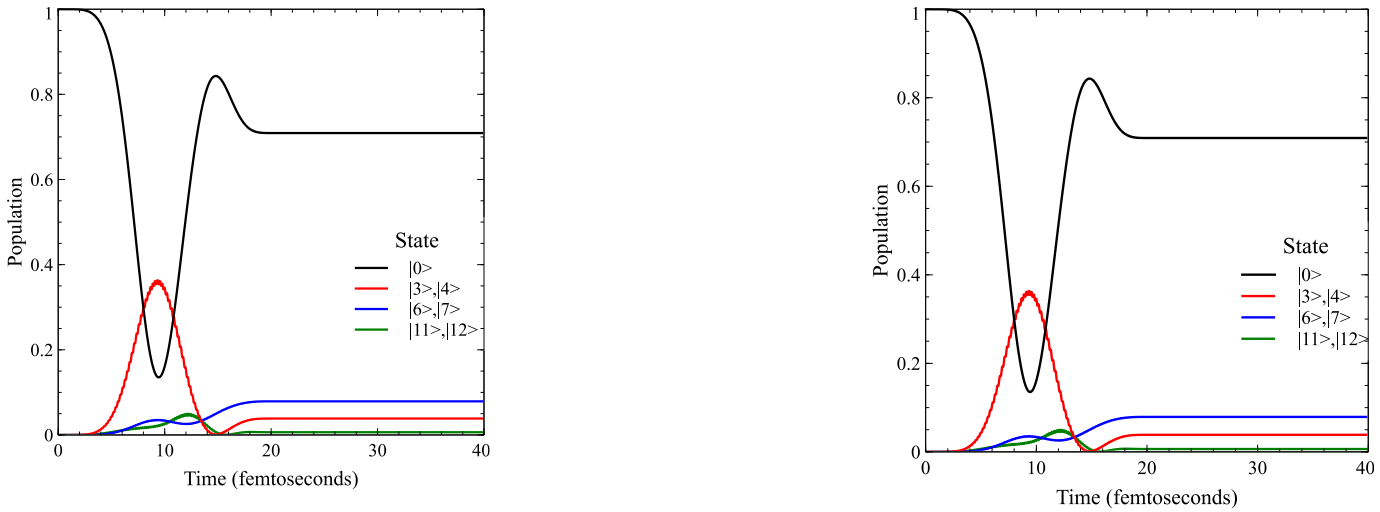

Figure S5(a). The variations of population of electronic states for the clockwise (CW) (left-panel) and counterclockwise (CCW) (right-panel) that are non-zero for the plane of circular laser pulse polarization *yz*. See the caption of **Figure 3(a)** for further details.

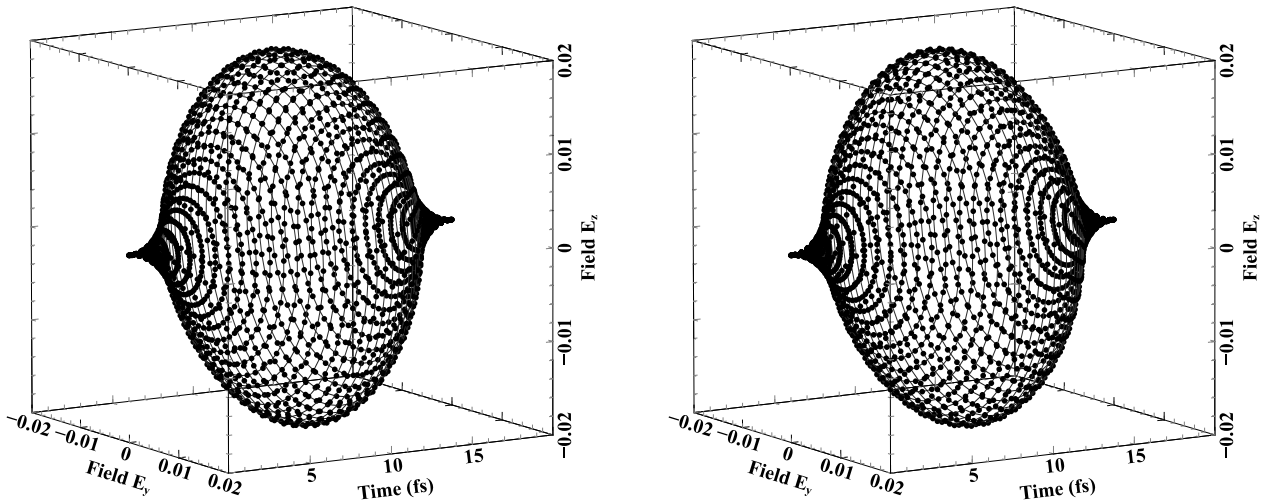

Figure S5(b). Time variations of the laser pulse electric field components $\mathbf{E_y}$, $\mathbf{E_z}$ for the *yz*-plane circular laser pulse polarization: clockwise (CW) (left-panel) and counterclockwise (CCW) (right-panel).

6. Supplementary Materials S6. Variations of the ethane C1-C2 *BCP* ellipticity ε for the right-handed (CW, [+1]) and left-handed (CCW, [-1]) circularly polarized laser pulse polarized in the *xz, xy* and *yz* planes.

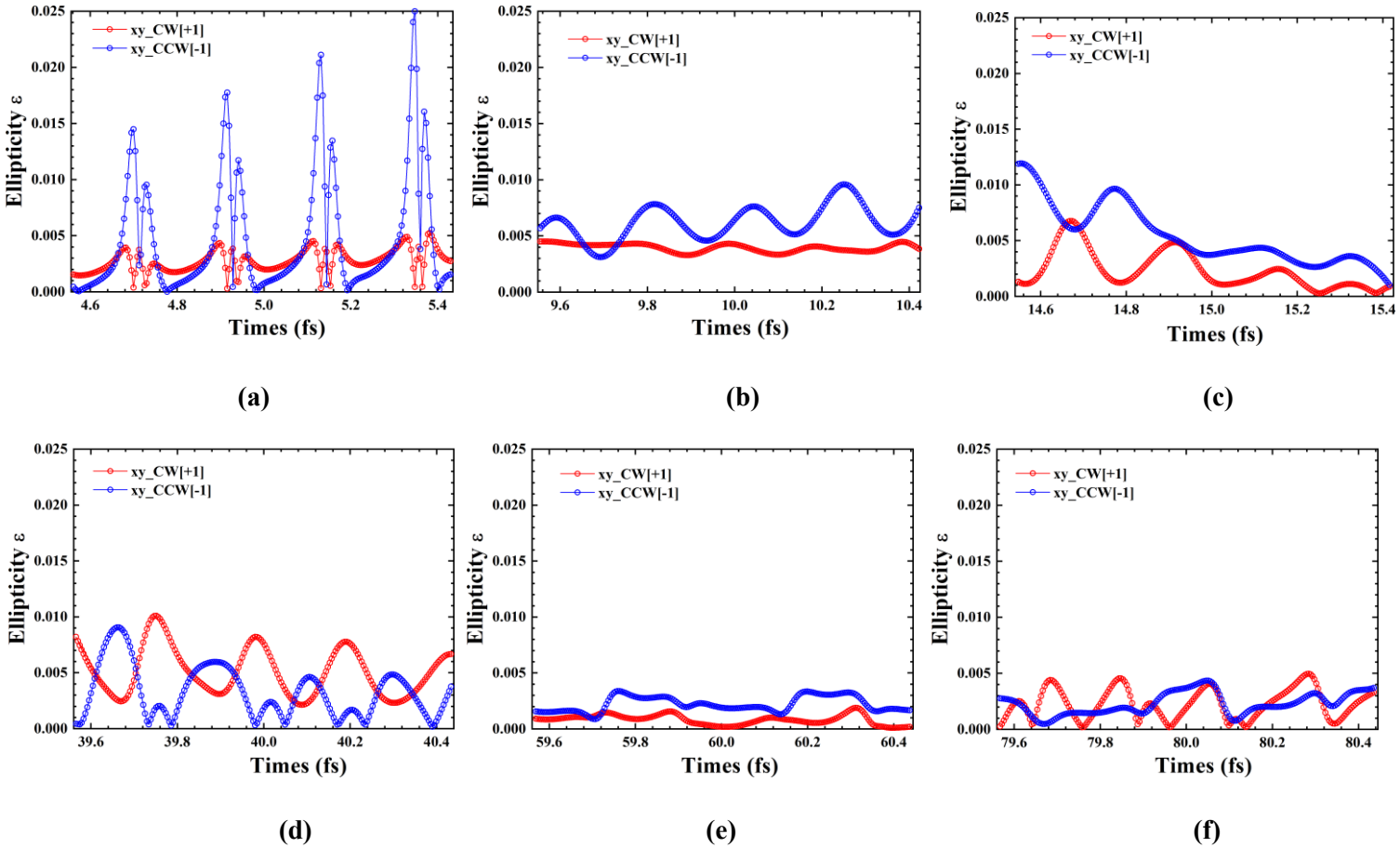

Figure S6(I). The variation of the ethane C1-C2 *BCP* ellipticity ε for the right-handed (**CW, [+1]**) and left-handed (**CCW, [-1]**) circularly polarized laser pulse polarized in the *xy* plane during the pulse at time t = 5 femtoseconds (fs), t =10 fs, t = 15 fs are presented in sub-figures **(a-c)** respectively. The corresponding plots after the pulse is switched off are presented at t = 40 fs, t = 60 fs and t = 80 fs in sub-figures **(d-f)** respectively.

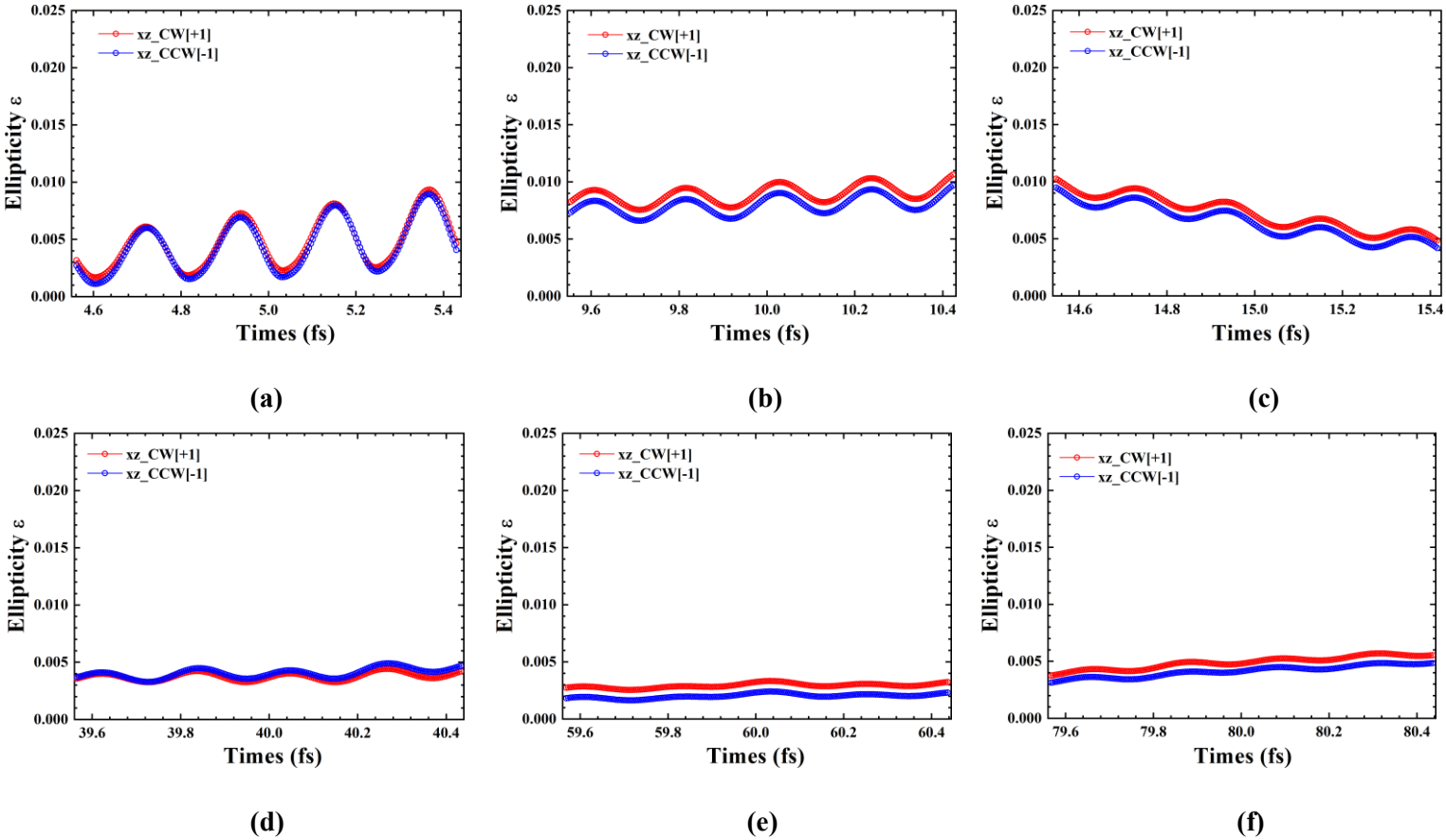

Figure S6(II). The variation of the ethane C1-C2 *BCP* ellipticity ε for the right-handed (CW, [+1]) and left-handed (CCW, [-1]) circularly polarized laser pulse polarized in the *xz* plane during the pulse at time t = 5 femtoseconds (fs), t =10 fs, t = 15 fs are presented in sub-figures **(a-c)** respectively. The corresponding plots after the pulse is switched off are presented at t = 40 fs, t = 60 fs and t = 80 fs in sub-figures **(d-f)** respectively.

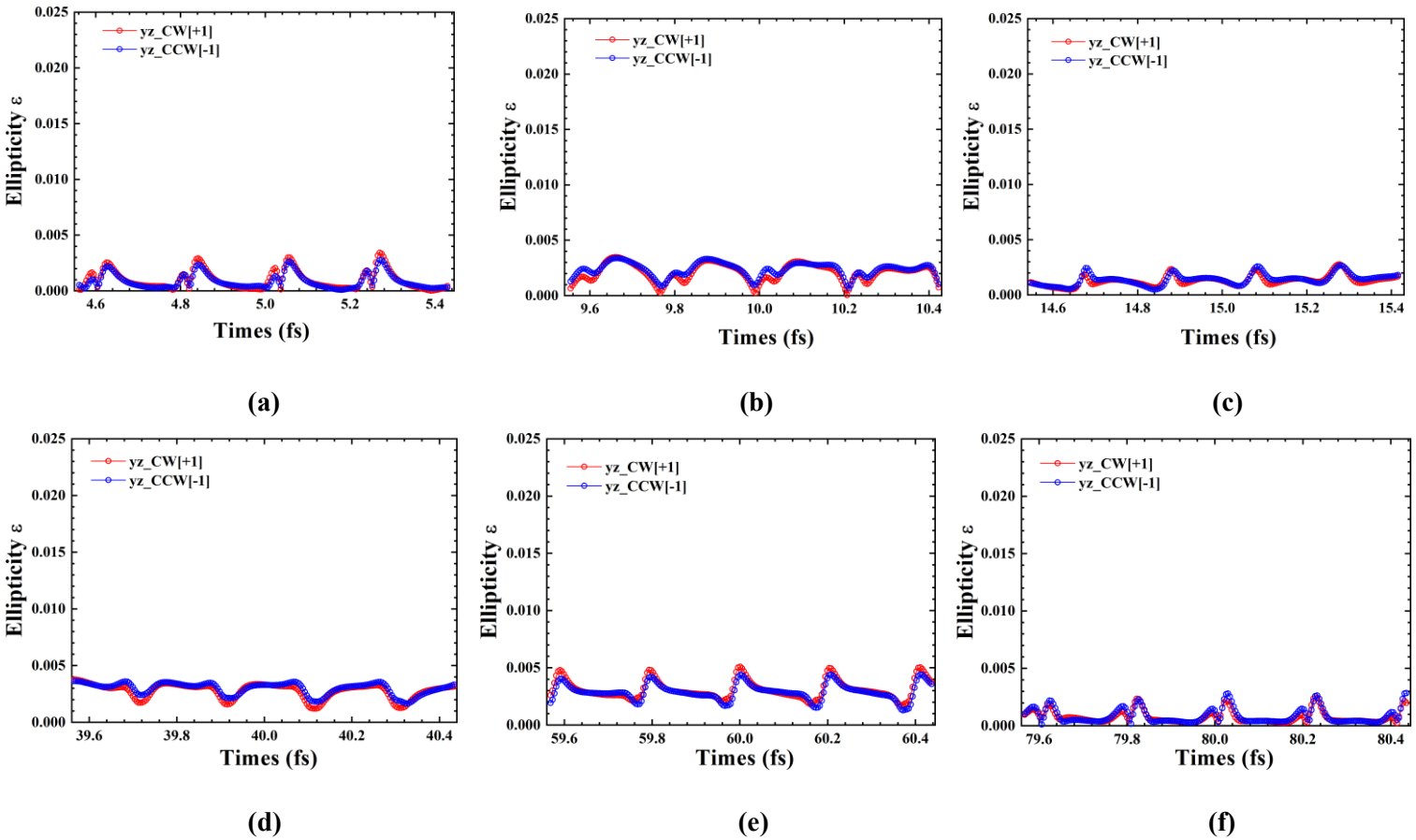

Figure S6(III). The variation of the ethane C1-C2 *BCP* ellipticity ε for the right-handed (CW, [+1]) and left-handed (CCW, [-1]) circularly polarized laser pulse polarized in the *yz* plane during the pulse at time t = 5 femtoseconds (fs), t =10 fs, t = 15 fs are presented in sub-figures **(a-c)** respectively. The corresponding plots after the pulse is switched off are presented at t = 40 fs, t = 60 fs and t = 80 fs in sub-figures **(d-f)** respectively.

7. Supplementary Materials S7. Maximum Hessian of $\rho(\mathbf{r})$ trajectory projections $\mathbb{T}_{max}(\boldsymbol{s})$ tables for the C1-C2 *BCP*s.

Table S7(a). The maximum Hessian of $\rho(\mathbf{r})$ trajectory projections $\mathbb{T}_{max}(\boldsymbol{s})$ = {bond-flexing$_{max}$, bond-twist$_{max}$, bond-axiality$_{max}$} where $\mathbb{F}$ = bond-flexing$_{max}$, $\mathbb{T}$ = bond-twist$_{max}$ and $\mathbb{A}$ = bond-axiality$_{max}$} of the C1-C2 *BCPs* of ethane corresponding to the right-handed CW (R, [+1]) and left-handed CCW (S, [-1]) planes of polarization *xy* are provided; all entries have been multiplied by 10^3.

	{$\mathbb{F}$, $\mathbb{T}$, $\mathbb{A}$ }	
	CW (R, [+1])	**CCW (S, [-1])**
During laser pulse		
t = 5	{1.273541, 0.009446, 4.439159}	{1.287508, 0.037298, 4.427183}
t = 10	{0.275696, 0.012894, 1.557779}	{0.010233, 0.277669, 1.548266}
t = 15	{0.321842, 0.032347, 2.225842}	{0.002958, 0.202199, 1.965551}
After laser pulse		
t = 40	{0.389028, 0.006964, 2.133914}	{0.307821, 0.175695, 1.904855}
t = 60	{0.005813, 0.752187, 1.380848}	{0.011018, 0.722225, 1.210264}
t = 80	{0.448935, 0.365426, 1.850161}	{0.029208, 0.626053, 1.632237}

Table S7(b). The $\mathbb{T}_{max}(\boldsymbol{s})$ of the C1-C2 *BCPs* of ethane corresponding to the CW (R, [+1]) and CCW (S, [-1]) planes of polarization *xz* are provided, see the caption of **Table S7(a)** for further details.

	{$\mathbb{F}$, $\mathbb{T}$, $\mathbb{A}$ }	
During laser pulse		
t = 5	{1.232053, 0.295792, 4.431031}	{1.247603, 0.221248, 4.431025}
t = 10	{0.145579, 0.135394, 1.391480}	{0.145956, 0.134883, 1.391443}
t = 15	{0.261370, 0.229909, 1.317836}	{0.260524, 0.230804, 1.317867}
After laser pulse		
t = 40	{0.287099, 0.047683, 1.453326}	{0.284105, 0.064219, 1.453410}
t = 60	{0.383197, 0.424733, 0.914224}	{0.406045, 0.402827, 0.914266}
t = 80	{0.417616, 0.250416,1.259808}	{0.437638, 0.213588, 1.259853}

Table S7(c). The $\mathbb{T}_{max}(\boldsymbol{s})$ of the C1-C2 *BCPs* of ethane corresponding to the CW (R, [+1]) and CCW (S, [-1]) planes of polarization *yz* are provided, see the caption of **Table S7(a)** for further details. Note for the *yz* plane of polarization we have chirality $\mathbb{C}$ instead of bond-twist $\mathbb{T}$ although the definitions are the same.

	$\{\mathbb{F}, \mathbb{C}, \mathbb{A}\}$	
During laser pulse		
$t = 5$	{1.222299, 1.224358, 0.028430}	{1.209301, 1.227912, 0.028439}
$t = 10$	{0.702646, 0.641314, 0.365793}	{0.711955, 0.649274, 0.365768}
$t = 15$	{1.322003, 1.195902, 1.109090}	{1.319895, 1.193734, 1.109129}
After laser pulse		
$t = 40$	{0.854347, 0.873736, 1.025006}	{0.854653, 0.874595, 1.025011}
$t = 60$	{1.274378, 1.268185, 1.031282}	{1.274928, 1.267756, 1.031374}
$t = 80$	{1.216450, 1.186798, 1.040782}	{1.218440, 1.185581, 1.040736}